http://dx.doi.org/10.5012/bkcs.2012.33.12.4098

Loss of HCN from the Pyrimidine Molecular Ion: A Computational Study

Min Kyoung Yim, Sun Hwa Jung, Myung Soo Kim,† and Joong Chul Choe*

*Department of Chemistry, Dongguk University-Seoul, Seoul 100-715, Korea. *E-mail: jcchoe@dongguk.edu*
†Department of Chemistry, Seoul National University, Seoul 151-742, Korea
Received August 31, 2012, Accepted September 25, 2012

The potential energy surface (PES) for the loss of HCN from the pyrimidine molecular ion has been explored using quantum chemical calculations. Possible reaction pathways to form five $C_3H_3N^{+\bullet}$ isomers have been obtained with Gaussian 4 model calculations. The rate constant for the HCN loss and the product branching ratio have been calculated using the Rice-Ramsperger-Kassel-Marcus theory on the basis of the obtained PES. The resultant rate constant agrees with the previous experimental result. By a kinetic analysis, it is proposed that the formation of $CH{=}CHC{\equiv}NH^{+\bullet}$ is favored near the dissociation threshold, while the formation of $CH{=}CHN{\equiv}CH^{+\bullet}$ is favored at high energies.

Key Words : G4 calculation, RRKM calculation, Kinetics, Reaction pathway

Introduction

Usually several competitive reactions occur in dissociations of polyatomic ions. When the ionic products are isomeric, their relative abundance cannot be determined by conventional mass spectrometry. Several experimental techniques based on tandem mass spectrometry have been developed to identify such isomeric products, which include the methods utilizing metastable ion dissociation, collision-induced dissociation, and ion-molecule reactions.[1-5] The relative abundance of isomeric products can be predicted through computational studies of the reaction mechanisms and kinetics together with their identification. For example, competitive formations of the isomeric benzylium and tropylium ions by the loss of $H^{\bullet}$ from the toluene molecular ion were extensively studied using both experimental and theoretical means.[4-7]

Recently, we have theoretically examined the competitive formations of $C_4H_4^{+\bullet}$ isomers by the loss of HCN from the pyridine molecular ion.[8] The study showed that the product branching ratio was determined by the reaction kinetics, not by the thermodynamics. It was predicted that the branching ratio of the main $C_4H_4^{+\bullet}$ products, the methylenecyclopropene and vinylacetylene radical cations, was varied dramatically on the internal energy. On the other hand, it was predicted that $CH{=}CHN{\equiv}CH^{+\bullet}$ was the predominant product among four possible $C_3H_3N^{+\bullet}$ isomers in the loss of HCN from the pyrazine (1,4-diazine) molecular ion in our successive study.[9]

In this work, we examined the dissociation of the pyrimidine (1,3-diazine) molecular ion (**1**, Figure 1) as a second attempt to study the reaction kinetics of three ionized diazine isomers. The 70 eV electron ionization (EI) mass spectra of pyrimidine and pyrazine are similar, whereas that of pyridazine (1,2-diazine) is different.[10] In the spectra of the former two isomers, the peaks corresponding to $[M - HCN]^{+\bullet}$ and $[M - 2HCN]^{+\bullet}$ are major fragment peaks, where M denotes the molecule. This suggests a possibility that the two isomers may dissociate *via* one or more common intermediates. In contrast, $[M - N_2]^{+\bullet}$, $[M - HN_2]^{+}$, and $[M - 2HCN]^{+\bullet}$ are major product ions in the dissociation of the pyridazine molecular ion by 70 eV EI. The dissociation of **1** has been studied using experimental methods such as charge exchange ionization,[11] photoionization,[12] photoelectron-photoion coincidence (PEPICO) spectroscopy,[13] and collision-induced dissociation.[14,15] In a PEPICO study by Buff and Dannacher,[13] the loss of HCN was the only dissociation channel, and the breakdown curves for the dissociation were fitted by a Rice-Ramsperger-Kassel-Marcus (RRKM)[16] model calculation. In a study of the reaction of the acrylonitrile ion ($CH_2{=}CHC{\equiv}N^{+\bullet}$) with HCN by Ervasti *et al.*,[15] the reaction pathways and energetics for the formation of **1** from several $C_3H_3N^{+\bullet}$ isomers with HCN were theoretically obtained. In this work, the potential energy surface (PES) for the formation of five possible $C_3H_3N^{+\bullet}$ isomers by the loss of HCN from **1** was obtained by Gaussian 4 (G4)[17] model calculations, based on the result of Ervasti *et al*. A kinetic analysis was performed to predict the dissociation rate constant and the product branching ratio.

Computational Methods

The molecular orbital calculations were performed using the Gaussian 09 program suite.[18] The geometries of the stationary points were optimized at the unrestricted B3LYP level of the density functional theory (DFT) using the 6-31G(d) basis set. The transition state (TS) geometries that connected the stationary points were examined and checked by calculating the intrinsic reaction coordinates at the same level. The G4 model calculations were performed for better accuracy of the energies. Two species, **10** and TS **21** → **22**, were not optimized in G4 calculations but were optimized in Gaussian 3 (G3) calculations using the B3LYP density functional method.[19]

The RRKM expression was used to calculate the rate constants for the unimolecular reaction steps because the RRKM formula for the microcanonical ensemble was mathematically equivalent to the formula in the statistical quasi-equilibrium theory that was developed for ionic dissociations:[16]

$$k(E) = \frac{\sigma N^{\ddagger}(E-E_0)}{h\rho(E)} \quad (1)$$

In this equation, E is the internal energy of the reactant, E_0 is the activation energy of the reaction, $N^{\ddagger}$ is the sum of the TS states, ρ is the density of the reactant states, σ is the reaction path degeneracy, and h is Planck's constant. $N^{\ddagger}$ and ρ were evaluated through a direct count of the states using the Beyer-Swinehart algorithm.[20] The E_0 values for the individual steps were obtained from the G4 or G3//B3LYP calculations and were used for RRKM calculations. Each normal mode of vibration was treated as a harmonic oscillator. The vibrational frequencies that were obtained from the B3LYP/6-31G(2df,p) calculations were scaled down by a factor of 0.9652.[21] For **10** and TS **21** → **22**, the vibrational frequencies obtained from the B3LYP/6-31G(d) calculations were scaled down by a factor of 0.9613.[21] The rate constants were calculated at 0 K, which means that rotational effects were ignored.

Results and Discussion

Figure 1 shows the optimized geometries of **1** and five possible product $C_3H_3N^{+\bullet}$ ions, CH_2=C=C=$NH^{+\bullet}$ (**p1**), (*E*)-CH=CHC≡$NH^{+\bullet}$ ((*E*)-**p2**), (*Z*)-CH=CHC≡$NH^{+\bullet}$ ((*Z*)-**p2**), CH=CHN≡$CH^{+\bullet}$ (**p3**), and CH_2=C=N=$CH^{+\bullet}$ (**p4**), formed by the loss of HCN with calculated relative energies of the product ions. The theoretical reaction pathways and energetics for the formation of these five product ions were reported by Ervasti *et al.*[15] Our obtained PESs generally agree with their results but we present more detailed (complete) pathways and the data for energies at 0 K, rather than enthalpies of formation at 298 K, for the purpose of RRKM calculations.

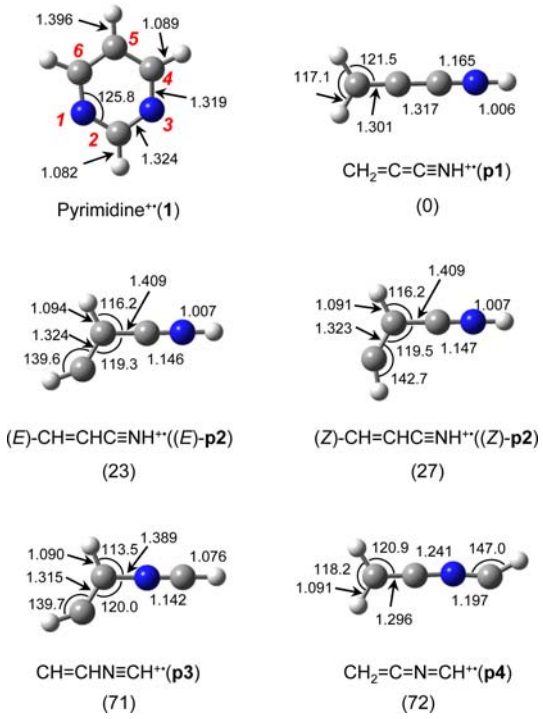

Figure 1. Geometric structures of **1** and $C_3H_3N^{+\bullet}$ isomers optimized by the G4 calculations. The numbers are the bond lengths in Å and the angles are in degree. The values in parentheses are relative energies of $C_3H_3N^{+\bullet}$ isomers in kJ mol^{-1}, obtained by the G4 calculations.

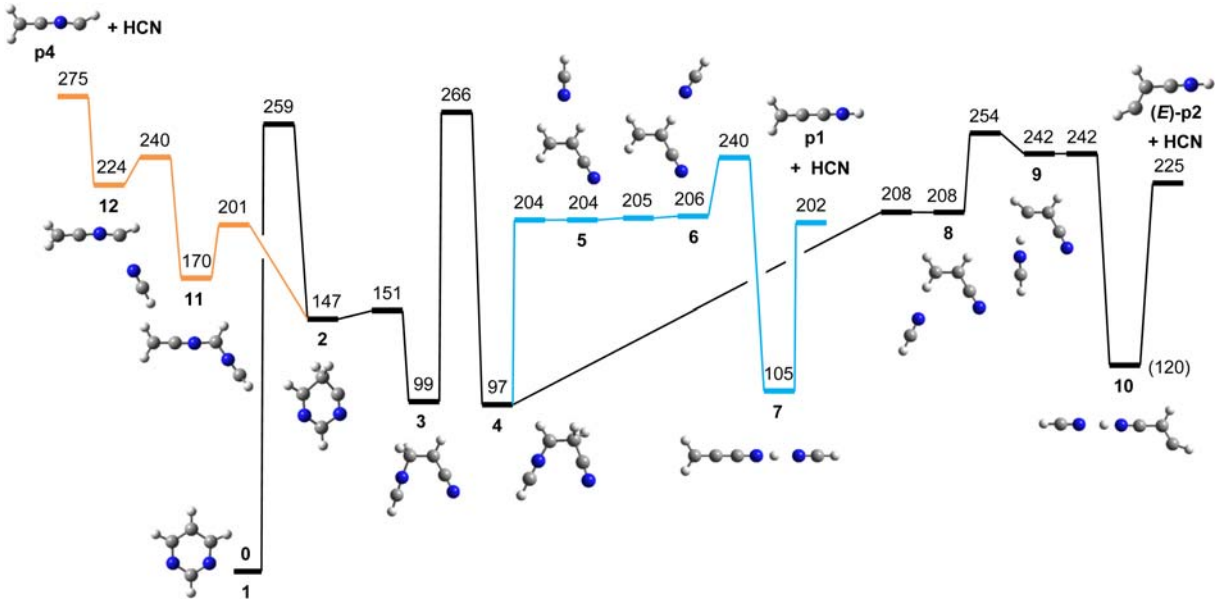

Figure 2. Potential energy diagram for the formation of **p1**, **p2**, and **p4** by the loss of HCN from **1**, derived from the G4 calculations. The energies are presented in kJ mol^{-1}. The calculated total energy of **1** was –263.8392761 hartrees. The energy of **10** was derived from the G3//B3LYP calculation because it was not optimized in the G4 calculation.

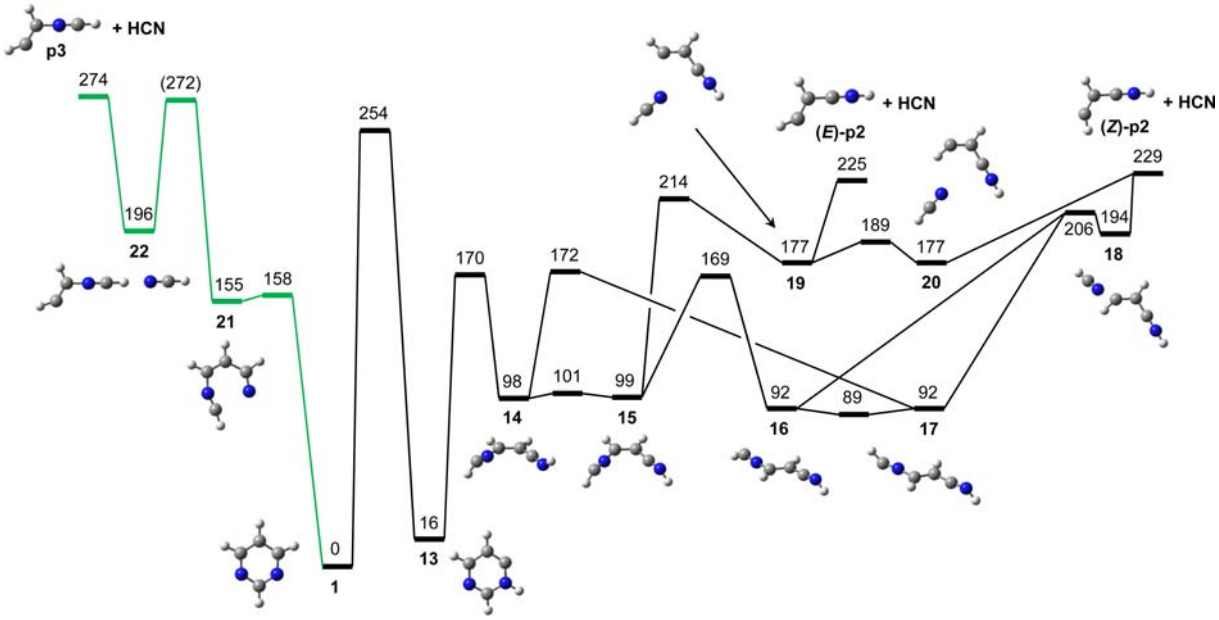

Figure 3. Potential energy diagram for the formation of **p2** and **p3** by the loss of HCN from **1**, derived from the G4 calculations. The energies are presented in kJ mol^{-1}. The energy of TS **21** → **22** was derived from the G3//B3LYP calculation because it was not optimized in the G4 calculation.

The PES for the formation of **p1**, **p2**, and **p4** is shown in Figure 2. The isomerization of **1** to **2** occurs by the shift of H on C4 to C5 (see Figure 1 for numbering). The C2–N3 bond of **2** is cleaved to form opened isomer **3**. Another 1,2-H shift forms the isomer **4**, and HCN is eliminated *via* three ion-molecule complexes to form **p1**, the most stable among the examined $C_3H_3N^{+\bullet}$ isomers. Alternatively, **4** can isomerize to other ion-molecule complexes, **8**, **9**, and **10**, followed by the loss of HCN to form (*E*)-**p2**. The cleavage of the C5–C6 bond of **2** leads to the formation of **p4** by the loss of HCN. The overall activation energies for the formation of **p1**, (*E*)-**p2**, and **p4** are 266, 266, and 275 kJ mol^{-1}, respectively.

p2 can be formed by other pathways shown in Figure 3. After the shift of H on C4 to N3 to form **13**, the C2–N3 bond is cleaved to form opened isomer **14**, which easily isomerizes to **15**. After a *cis-trans* isomerization to form **16**, HCN is eliminated to form (*Z*)-**p2** *via* ion-molecule complex **18**. Alternatively, the formation of (*Z*)-**p2** can occur after the *cis-trans* isomerization of **14** → **17**. (*E*)-**p2** can be formed from **15** by the loss of HCN *via* **19**. The isomerization **19** → **20** leads to the formation of (*Z*)-**p2**. The cleavage of the C2–N3 bond of **1** eventually forms **p3** by the loss of HCN *via* **21** and **22**. The overall activation energies for the formation of (*Z*)-**p2**, (*E*)-**p2**, and **p3** along these pathways are 254, 254, and 274 kJ mol^{-1}, respectively. Our calculations suggest that the formation of **p2** is energetically the most favored among the HCN loss channels. However, because the overall activation energies are not largely different, the entropic factor can be important in the dissociation kinetics.

The isomerization **1** → **2** is the key step for the formation of **p1**, **p2**, and **p4** (Figure 2), and **1** → **13** and **1** → **22** are those of **p2** and **p3** (Figure 3), respectively. We ignore **21** in the last step because its presence does not affect the rate for the formation of **p3**. The energy dependence of the rate constants, $k(E)$, calculated using the RRKM formalism for these three key steps are shown in Figure 4. k(**1** → **13**) is largest near the dissociation threshold. However, at energies higher than 290 kJ mol^{-1}, k(**1** → **22**) is the largest, and the slope of its energy dependence is the steepest, indicating that the corresponding TS is looser than the other two TSs. The looseness of a TS is usually evaluated by activation entropy ($\Delta S^{\ddagger}$),[16] which is calculated from geometries of the reactant and TS in a reaction step. The larger $\Delta S^{\ddagger}$ is, the looser the TS is. The $\Delta S^{\ddagger}$ value at 1000 K calculated for the reaction **1** → **22**, 68 J mol^{-1} K^{-1}, is much larger than those calculated for the reactions **1** → **13** and **1** → **2**, which are 9 and −1 J mol^{-1} K^{-1}, respectively. The resultant $k(E)$ curves in Figure 4 sug-

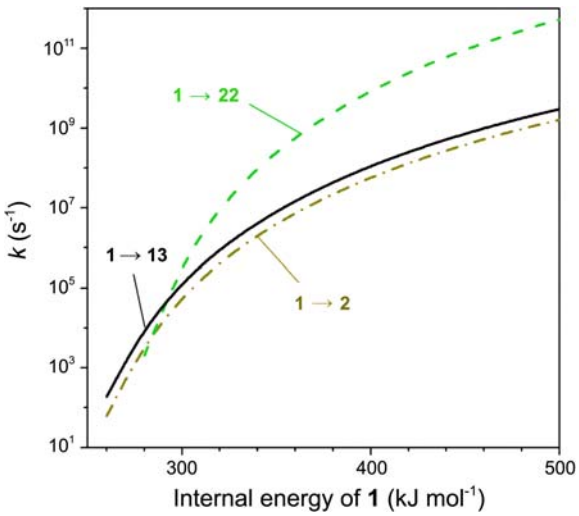

Figure 4. RRKM energy dependences of the rate constants for **1** → **2**, **2** → **13**, and **1** → **22**.

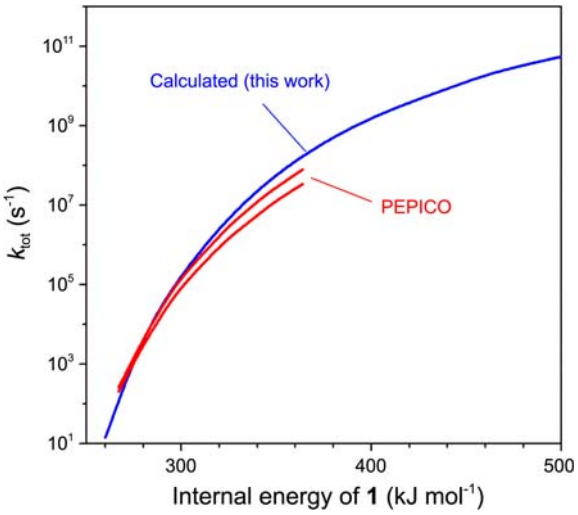

Figure 5. Theoretical and experimental energy dependences of the rate constant for the loss of HCN from **1**. The PEPICO data by Buff and Dannacher[13] were obtained, so that the experimental breakdown curves measured at ion source residence times of 1 and 6 μs achieved best fits by calculations that used the RRKM $k_{HCN}(E)$ curves. The results are presented as the lower and upper lines, respectively.

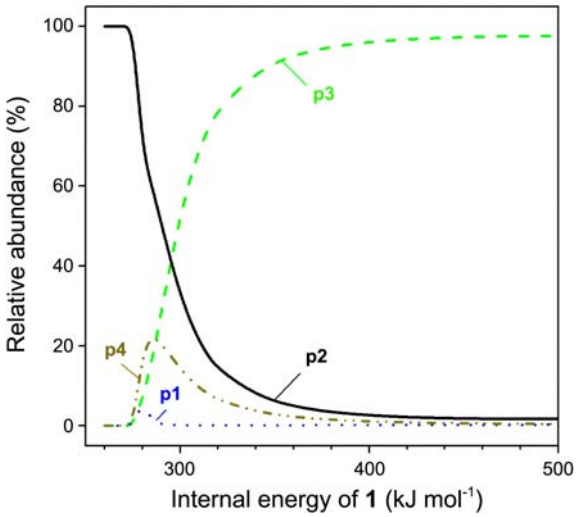

Figure 6. Theoretical abundances of **p1-p4** formed by the loss of HCN from **1**.

gest that near the threshold, the formation of **p2** is the most favored, while at higher energies, the formation of **p3** is the most favored. However, the next steps can affect the dissociation kinetics.

For a more detailed kinetic analysis, the total rate constant for the HCN loss, k_{tot}, and the product branching ratio were calculated by solving the coupled differential equations for the rate laws of the individual dissociation channels. MATLAB software was used to numerically solve the coupled differential equations. The solution provided the time dependence of the concentrations of **1**, the intermediates, and the products at a specific ion internal energy. k_{tot} was obtained by fitting an exponential law to the sum of the time dependences of the concentrations of **1** and all the intermediates. The branching ratios of **p1-p4** were obtained from the time dependences of their concentrations. This procedure was repeated for a range of the internal energy values.

The individual rate constants for the reaction steps in Figures 2 and 3, which were used in the calculations of k_{tot} and the branching ratio, were calculated using the RRKM formalism. All the final dissociation steps proceed through "loose" TSs that could not be located. For the calculations of their rate constants, activation entropy was used. For the dissociation steps, the frequencies for each loose TS were adjusted so that $\Delta S^{\ddagger}$ at 1000 K might be 24 J mol^{-1} K^{-1} because most of the reported $\Delta S^{\ddagger}_{1000K}$ values for the bond cleavages *via* a loose TS are in the range of 13-35 J mol^{-1} K^{-1}.[8]

The resultant energy dependences of k_{tot} and the branching ratio are shown in Figures 5 and 6, respectively. The calculated $k_{tot}(E)$ agrees with the previous PEPICO experimental results,[13] obtained by fitting the breakdown curves, within the experimental error limit. Figure 6 shows that **p2** is the most abundant near the reaction threshold, while **p3** is the most abundant at the energies higher than 295 kJ mol^{-1}, corresponding to $k_{tot} = 8 \times 10^4$ s^{-1}. This agrees with the above prediction based on Figure 4. It is predicted that **p4** is the third most abundant over the entire range of energies investigated, and the abundance of **p1**, the most stable among examined $C_3H_3N^{+\bullet}$ ions, is negligible. Therefore, at the usual metastable windows corresponding to $k = 10^5$-10^6 s^{-1}, the product abundance is predicted to be [**p3**] > [**p2**] > [**p4**]. The ratio of (*Z*)- and (*E*)-**p2** depends on the energy. Near the threshold, (*Z*)-**p2** is much more abundant, and as the energy increases, the relative abundance of (*E*)-**p2** increases. The calculated *Z* to *E* ratios are 22, 13, and 5.9 at the energies of 260, 300, and 340, respectively.

Conclusion

The kinetic analysis for the loss of HCN from **1** shows that the rate constant agrees with the previous PEPICO result and the most favorable products are **p2** near the threshold and **p3** at high energies. The formation of other $C_3H_3N^{+\bullet}$ isomers is less important. The formation of **p3** starts by C–N bond cleavage through a loose TS, while the formation of **p2** starts by a 1,2-H shift through a tight TS. As a result, the former reaction is more favored at high energies, even though it is thermodynamically less favored than the latter.

Acknowledgments. This work was supported by the National Research Foundation of Korea Grant funded by the Korean Government (2010-0008287).

References

1. Levsen, K. In *Fundamental Aspects of Organic Mass Spectrometry*; Verlag Chemie: Weinheim, 1978.
2. Busch, K. L.; Glish, G. L.; McLuckey, S. A. *Mass Spectrometry/ Mass Spectrometry: Techniques and Applications of Tandem Mass Spectrometry*; VCH Publishers: New York, 1988.
3. Fati, D.; Lorquet, A. J.; Locht, R.; Lorquet, J. C.; Leyh, B. *J. Phys.*

Chem. A **2004**, *108*, 9777.
4. Moon, J. H.; Choe, J. C.; Kim, M. S. *J. Phys. Chem. A* **2000**, *104*, 458.
5. Huang, F. S.; Dunbar, R. C. *Int. J. Mass Spectrom. Ion Processes* **1991**, *109*, 151.
6. Lifshitz, C. *Acc. Chem. Res.* **1994**, *27*, 138.
7. Choe, J. C. *J. Phys. Chem. A* **2006**, *110*, 7655.
8. Yim, M. K.; Choe, J. C. *J. Phys. Chem. A* **2011**, *115*, 3087.
9. Jung, S. H.; Yim, M. K.; Choe, J. C. *Bull. Korean Chem. Soc. 32*, 2301.
10. *NIST Chemistry WebBook*, NIST Standard Reference Database Number 69.
11. Åsbrink, L.; Fridh, C.; Jonsson, B. Ö.; Lindholm, E. *Intern. J. Mass Spectrom. Ion Phys.* **1972**, *8*, 215.
12. Vall-Llosera, G.; Coreno, M.; Erman, P.; Huels, M.; Jakubowska, K.; Kivimaki, A.; Rachlew, E.; Stankiewicz, M. *Int. J. Mass Spectrom.* **2008**, *275*, 55.
13. Buff, R.; Dannacher, J. *Int. J. Mass Spectrom. Ion Processes* **1984**, *62*, 1.
14. Lavorato, D. J.; Dargel, T. K.; Koch, W.; McGibbon, G. A.; Schwarz, H.; Terlouw, J. K. *Intern. J. Mass Spectrom.* **2001**, *210*, 43.
15. Ervasti, H. K.; Jobst, K. J.; Gerbaux, P.; Burgers, P. C.; Ruttink, P. J. A.; Terlouw, J. K. *Chem. Phys. Let.* **2009**, *482*, 211.
16. Baer, T.; Hase, W. L. *Unimolecular Reaction Dynamics: Theory and Experiments*; Oxford University Press: New York, 1996.
17. Curtiss, L. A.; Redfern, P. C.; Raghavachari, K. *J. Chem. Phys.* **2007**, *126*, 084108.
18. Frisch, M. J. T., Trucks, G. W.; Schlegel, H. B.; Scuseria, G. E.; Robb, M. A.; Cheeseman, J. R.; Scalmani, G.; Barone, V.; Mennucci, B.; Petersson, G. A.; Nakatsuji, H.; Caricato, M.; Li, X.; Hratchian, H. P.; Izmaylov, A. F.; Bloino, J.; Zheng, G.; Sonnenberg, J. L.; Hada, M.; Ehara, M.; Toyota, K.; Fukuda, R.; Hasegawa, J.; Ishida, M.; Nakajima, T.; Honda, Y.; Kitao, O.; Nakai, H.; Vreven, T.; Montgomery, J. A., Jr.; Peralta, J. E.; Ogliaro, F.; Bearpark, M.; Heyd, J. J.; Brothers, E.; Kudin, K. N.; Staroverov, V. N.; Kobayashi, R.; Normand, J.; Raghavachari, K.; Rendell, A.; Burant, J. C.; Iyengar, S. S.; Tomasi, J.; Cossi, M.; Rega, N.; Millam, N. J.; Klene, M.; Knox, J. E.; Cross, J. B.; Bakken, V.; Adamo, C.; Jaramillo, J.; Gomperts, R.; Stratmann, R. E.; Yazyev, O.; Austin, A. J.; Cammi, R.; Pomelli, C.; Ochterski, J. W.; Martin, R. L.; Morokuma, K.; Zakrzewski, V. G.; Voth, G. A.; Salvador, P.; Dannenberg, J. J.; Dapprich, S.; Daniels, A. D.; Farkas, Ö.; Foresman, J. B.; Ortiz, J. V.; Cioslowski, J.; Fox, D. J. *Gaussian 09, revision A. 02*; Gaussian, Inc., Wallingford CT, 2009.
19. Baboul, A. G.; Curtiss, L. A.; Redfern, P. C. *J. Chem. Phys.* **1999**, *110*, 7650.
20. Beyer, T.; Swinehart, D. R. *ACM Commun.* **1973**, *16*, 379.
21. Merrick, J. P.; Moran, D.; Radom, L. *J. Phys. Chem. A* **2007**, *111*, 11683.